View metadata, citation and similar papers at core.ac.uk

brought to you by CORE

provided by Warwick Research Archives Portal Repository

Original citation:
Frisk, Andreas, Hase, Thomas P. A., Svedlindh, Peter, Johansson, Erik and Andersson, Gabriella. (2017) Strain engineering for controlled growth of thin-film FeNi L10. Journal of Physics D: Applied Physics, 50 (8). 085009.

Permanent WRAP URL:
http://wrap.warwick.ac.uk/85856

Copyright and reuse:
The Warwick Research Archive Portal (WRAP) makes this work by researchers of the University of Warwick available open access under the following conditions. Copyright © and all moral rights to the version of the paper presented here belong to the individual author(s) and/or other copyright owners. To the extent reasonable and practicable the material made available in WRAP has been checked for eligibility before being made available.

Copies of full items can be used for personal research or study, educational, or not-for-profit purposes without prior permission or charge. Provided that the authors, title and full bibliographic details are credited, a hyperlink and/or URL is given for the original metadata page and the content is not changed in any way.

Publisher's statement:
This is an author-created, un-copyedited version of an article published in Journal of Physics D: Applied Physics. IOP Publishing Ltd is not responsible for any errors or omissions in this version of the manuscript or any version derived from it. The Version of Record is available online at https://doi.org/10.1088/1361-6463/aa5629

A note on versions:
The version presented here may differ from the published version or, version of record, if you wish to cite this item you are advised to consult the publisher's version. Please see the 'permanent WRAP URL' above for details on accessing the published version and note that access may require a subscription.

For more information, please contact the WRAP Team at: wrap@warwick.ac.uk

warwick.ac.uk/lib-publications

Strain Engineering for Controlled Growth of Thin-Film FeNi $L1_0$

Andreas Frisk[1]‡, Thomas P.A. Hase[2], Peter Svedlindh[3], Erik Johansson[4] and Gabriella Andersson[1]

[1] Department of Physics and Astronomy, Uppsala University, Box 516, SE-751 20 Uppsala, Sweden
[2] Department of Physics, University of Warwick, Coventry, CV4 7AL, United Kingdom
[3] Department of Engineering Sciences, Uppsala University, Box 537, SE-751 20 Uppsala, Sweden
[2] ABB AB, Power Devices, Corporate Research, SE-721 78 Västerås, Sweden

Abstract. FeNi thin films in the $L1_0$ phase were successfully grown by magnetron sputtering on HF-etched Si(001) substrates on $Cu/Cu_{100-x}Ni_x$ buffers. The strain of the FeNi layer, $(c/a)_{FeNi}$, was varied in a controlled manner by changing the Ni content of the $Cu_{100-x}Ni_x$ buffer layer from $x = 0$ at.% to $x = 90$ at.%, which influenced the common in-plane lattice parameter of the CuNi and FeNi layers. The presence of the $L1_0$ phase was confirmed by resonant x-ray diffraction measurements at various positions in reciprocal space. The uniaxial magnetocrystalline anisotropy energy K_U is observed to be smaller (around $0.35\,MJ\,m^{-3}$) than predicted for a perfect FeNi $L1_0$ sample, but it is larger than for previously studied films. No notable variation in K_U with strain state $(c/a)_{FeNi}$ is observed in the range achieved ($0.99 \lesssim (c/a)_{FeNi} \lesssim 1.02$), which is in agreement with theoretical predictions.

PACS numbers: 61.05.cp, 75.30.Gw, 75.70.Ak

‡ Corresponding author: andreas.frisk@physics.uu.se

1. Introduction

Modern technology requires access to materials with a wide range of tunable properties that can be readily incorporated into relevant sample architectures. Many functional systems contain room temperature ferromagnetic materials which, for certain applications, also require a high uniaxial anisotropy, K_U. High K_U materials can be engineered by alloying rare-earth and transition metal elements [1]. However, with the high financial and environmental costs of such alloys, there has recently been a drive to find new high K_U systems composed of only transitional metal elements [2, 3, 4]. A potentially useful material is FeNi in the L1$_0$ ordered structure in which the Fe and Ni atoms are arranged in alternating layers within a face centred cubic unit cell (fig. 1, inset). The magnetic properties of the L1$_0$ phase are believed to originate from the chemical and structural anisotropy [5, 6, 7, 8, 9, 10, 11], with an ideal FeNi L1$_0$ unit cell being slightly tetragonally strained with $c/a = 1.006$ [5]. However stabilizing the L1$_0$ structure is not trivial with thermally driven diffusion introducing Fe/Ni site disorder with a concomitant degradation in the desired magnetic properties [12].

Since the FeNi L1$_0$ phase was first discovered in the 1960s [13], various methods have been attempted to obtain this thermodynamically stable structure. Bulk crystals have been produced by neutron bombardment [14], electron irradiation [15] or in small amounts by severe plastic deformation [16] as well as direct chemical processes [17]. More recently, advances in thin film deposition have opened up new routes to incorporating epitaxial L1$_0$ FeNi in artificial heterostructures through elemental layer-by-layer growth [18, 9, 19].

When considering epitaxial growth of thin films for possible device applications, the choice of an industrially relevant substrate such as Si or GaAs significantly increases the range of technologies that can be impacted. However, to achieve epitaxial growth there must be a good structural match between the substrate and film. Mismatch between the substrate and overlayer can sometimes be overcome through the choice of suitable buffer layer(s) to create virtual substrates, a technique widely exploited in the semiconductor industry. Even so, additional post-growth treatment may still be required to achieve the desired crystal structure or phase. In L1$_0$ FePt or CoPt, post growth annealing is used regularly to reduce substitutional defects and enhance the layer-by-layer perfection [20, 21, 22]. However, in FeNi L1$_0$ any post-growth annealing has the opposite effect, namely promoting site disorder and destroying the layer-by-layer arrangement of the Fe and Ni atoms [12]. Thus, for FeNi, the L1$_0$ phase needs to be stabilized during growth and this requires careful consideration of the stoichiometry, composition, roughness and layer thickness of the buffer layer(s) as these can be used to engineer the strain in any subsequent overlayer. The importance of strain within FeNi L1$_0$ is exemplified in studies by Miura *et al.* [23], which suggest that K_U depends on the structural anisotropy which increases with the c/a ratio. We note that this effect has yet to be confirmed systematically through experiments.

In our previous study we demonstrated the possibility of synthesizing epitaxial thin films of L1$_0$ FeNi using alternating monolayer (ML) deposition of Fe and Ni via magnetron sputtering [24]. To achieve the desired film structure we chose a Cu buffered Si(001) substrate which in turn produced FeNi films with tensile in-plane strain, i.e. $c/a < 1$. The uniaxial anisotropy energy K_U we achieved in these Cu-buffered thin film samples was unfortunately lower than expected, which we attributed to a combination of roughness from the Cu buffer layer and the non-optimal strain state within the L1$_0$ film.

In this article, we explore the choice of a combined Cu/Cu$_{100-x}$Ni$_x$ buffer layer to tailor the strain state in L1$_0$ FeNi. We will demonstrate, using x-ray diffraction, how the the strain states can be engineered in the system through fine tuning of the in-plane lattice parameters via changes in the CuNi composition. This allows systematic investigation of the dependence of magnetic properties, especially the anisotropy K_U, on the c/a ratio inside the FeNi layer.

2. Experimental details

FeNi thin films were deposited using magnetron sputtering on Si(001) etched by hydrofluoric acid as described previously [24]. The base pressure of the growth chamber was 5.7×10^{-9} torr and an Ar sputtering gas pressure of 2×10^{-3} torr was used. The nominal structure of the films is shown in fig. 1. An initial Cu buffer layer of 1000 Å was deposited at room temperature on the pre-etched hydrogen terminated Si surface resulting in an epitaxial Cu layer with the [001] direction normal to the surface. The Cu buffer

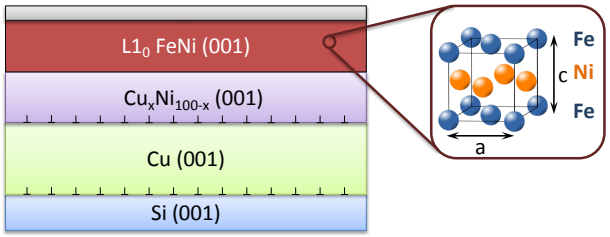

Figure 1. Nominal sample structure: a Si 001 substrate with Cu (1000 Å) and $Cu_{100-x}Ni_x$ (700 Å) buffer layers, on top of which a ∼ 360 Å FeNi film was deposited. Oxidation protection is provided by a sacrificial 20 Å Ni layer. Inset: The $L1_0$ phase within the FeNi layer ideally consists of alternating monolayers of Ni and Fe within a slightly tetragonally strained fcc unit cell with $c \gtrsim a$.

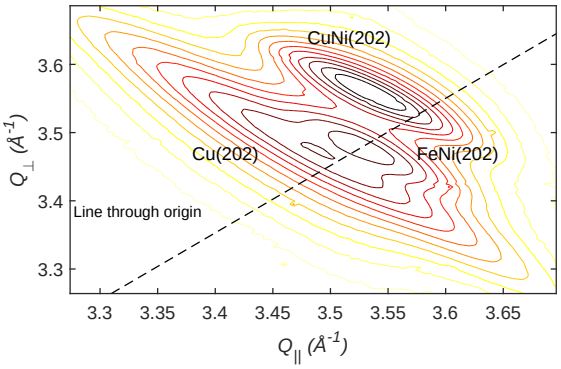

Figure 2. Reciprocal space map measured with 7120 eV radiation in the vicinity of the Cu, FeNi and CuNi (202) reflections from the 70 at.% Ni sample. $Q_\perp \parallel [0\,0\,1]$ is perpendicular and $Q_\parallel \parallel [1\,0\,0]$ is parallel to the sample surface. The CuNi, Cu and FeNi peaks are labelled, and the dashed line goes through the origin and the centre of the FeNi peak. $c_{\mathrm{FeNi}} > c_{\mathrm{CuNi}}$ since the CuNi peak lies above the line, while $a_{\mathrm{FeNi}} \approx a_{\mathrm{CuNi}}$ since both peaks have similar $Q_\parallel$ positions.

layer was subsequently annealed for 1 h at 150 °C after which a 700 Å thick CuNi layer was deposited at the same temperature. A series of samples with different $Cu_{100-x}Ni_x$ buffers with Ni content x ranging from 0 to 90 at.% was fabricated. The Fe and Ni alternating layers were deposited epitaxially onto the CuNi buffer at 150 °C: nominally 1 monolayer (ML) of Ni followed by 1 ML of Fe, repeated 100 times, resulting in a $L1_0$ FeNi layer of 200ML (∼360 Å) thickness. A deposition rate of 0.66 Å s^{-1} was used for the Cu layer, whilst the CuNi layer deposition rate varied between 0.21–1.16 Å s^{-1} depending upon composition. For the FeNi layer, a deposition rate of 0.136 Å s^{-1} (or 0.076 ML s^{-1}) was used for each element. To protect the films from oxidation a 20 Å Ni cap layer was deposited which transformed into a passivating NiO layer of about 15 Å after being exposed to air [25]. Using the same growth conditions, an additional control sample was grown in which the Fe and Ni were co-deposited to produce a film of similar thickness but in the chemically disordered A1 phase. Additional samples containing only the Cu and CuNi buffer layers (for a few selected CuNi compositions) were also grown to both aid the structural analysis and to provide calibration samples for the magnetometry.

Structural investigation of the samples was performed at room temperature using resonant X-ray diffraction on the XMaS beamline (BM28) at the ESRF [26]. A Si (111) monochromator selected linearly polarized light, from the bending magnet source, with energies in the vicinity of the Fe, Ni and Cu K absorption edges, 7080–9025 eV. The beamline was operated in a high resolution double axis setting with the reciprocal space resolution defined by narrow vertical slits used to define the incident and exit beams. Nitrogen was flowed continuously over the sample surface to prevent damage from ozone produced by the high intensity synchrotron beam. An energy resolved Vortex detector was used to discriminate the elastic scattering from the fluorescence background. Different regions of interest were defined in software from the energy resolved detector signal and integrated as separate scalars facilitating the efficient removal of the fluorescent background at the different energies used. Symmetric and asymmetric scans were performed in reciprocal space along directions defined using an optimised UB matrix [27]. In addition, energy scans at fixed scattering vector were used to confirm which of the overlapping peaks corresponded to the Cu, CuNi and FeNi layers. Supporting atomic force microscope (AFM) measurements in contact mode were made using a Nanosurf Mobile S system.

The magnetic properties of the samples were determined using a Quantum Design MPMS XL Superconducting Quantum Interference Device (SQUID). A reciprocating sample option head was used to measure the magnetic field dependent magnetization as well as the saturation magnetization M_S. Both in-plane and out-of-plane hysteresis loops were recorded at 300 K. By subtracting the measured magnetic moment from separate buffer reference samples consisting of only Cu/CuNi (see below), the magnetic properties of the FeNi layer could be isolated and correlated with the structural data.

3. Results and discussion

3.1. Structural Properties

Our choice of buffer layers, their thickness and thermal annealing protocols were motivated by the need to provide a smooth surface with an appropriate lattice parameter onto which the $L1_0$ FeNi layer could be grown. The buffer layers were designed to be

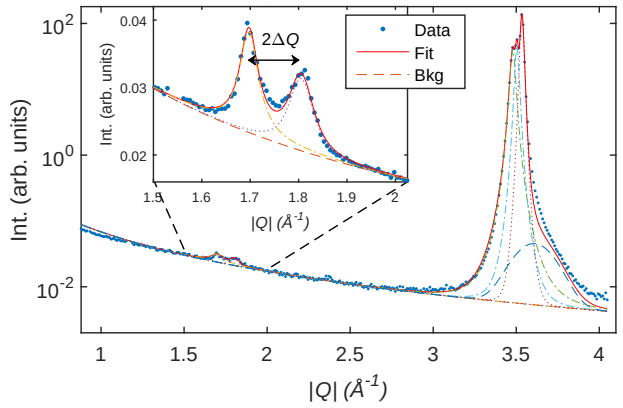

Figure 3. Scan along the [001] direction for the 40 at.% Ni sample with 7090 eV synchrotron radiation. Fits (lines) to the data (points) are shown for all peaks and the background. The (002) reflections of Cu, FeNi and CuNi are seen at $|Q| \approx 3.5$ Å^{-1}. Inset: A finer scan over the 001 reflections at $|Q| \approx 1.75$ Å^{-1}close to the Fe resonance (7120 eV) to enhance intensity. The sample shows a clearly split (001) reflection, with $\Delta Q = 0.054$ Å^{-1}.

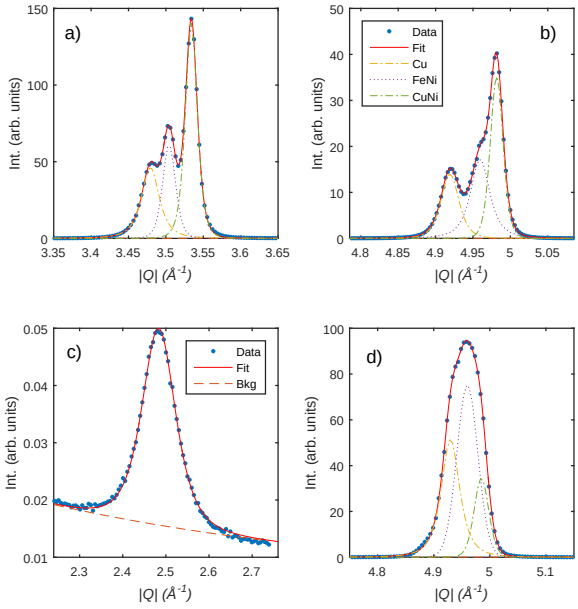

Figure 4. Scans along around the (002), (202), (110) (220) positions (a through d respectively) for the 40 at.% Ni sample recorded with an energy just below the Ni edge (8310 eV). The (002), (202) and (220) scans contains overlapping reflections from the Cu, FeNi and CuNi layers with the fitted peaks shown. In (c) the (110) reflection only contains the FeNi reflection which is fitted to a single peak. All scans are aligned to the FeNi reflection except for (a) which is aligned on the CuNi peak.

sufficiently thick to ensure that they had fully relaxed relative to the underlying layers. The successful epitaxial growth of each sample was confirmed by x-ray diffraction. Only expected reflections were observed, at positions close to those corresponding to relaxed lattice parameters of each of the layers. Fig. 2 shows the reciprocal space map (RSM) of diffracted intensity in the vicinity of the (202) peaks for the 70 at.% Ni sample, recorded after alignment to the FeNi peak. The symmetry of the peaks show that the layers have a uniform lattice parameter and the buffer layers are fully relaxed, with FeNi and CuNi sharing the same in-plane lattice parameter ($a_{\mathrm{FeNi}} \approx a_{\mathrm{CuNi}}$) but having different out-of-plane lattice parameters ($c_{\mathrm{FeNi}} > c_{\mathrm{CuNi}}$). Although the peaks are slightly overlapping we can estimate the in-plane coherence length to be 500 Å to 600 Å for the CuNi and FeNi layers. These sizes are similar to islands on top of Cu buffer layers which have been observed by atomic force microscopy both by ourselves and others [24, 28]. On addition of a CuNi buffer layer the roughness increases from ∼4 Å to a root mean squared value of about 10 Å on top of the 40 at.% Ni buffer reference sample. Although the errors are relatively large using AFM (∼5 Å), we believe this value to be representative for all samples studied and is consistent with transition metal layers grown using sputtering. We cannot, however, rule out small variations in the surface roughness for the different $Cu_{100-x}Ni_x$ buffer layers [24].

The poor resolution of the reciprocal space map precludes precise measurement of the lattice parameters of the layers. Thus, these maps were not used for this purpose, but instead high resolution one-dimensional scans were performed along principal directions in reciprocal space after optimising on the peak of interest. Scans were performed along the [001],[110] and [101] directions. As an example the FeNi [101] scan is equivalent to tracking along the dashed line in fig. 2. For the chemically disordered A1 phase the (001) and (110) reflections are forbidden, and their appearance in measurements is often used as direct evidence of the $L1_0$ phase. The ratio of the peak intensities, (001)/(002) or (110)/(220), then defines an order parameter relevant to the degree of $L1_0$ order [29]. An additional confirmation of $L1_0$ order can be sought by measuring the peak intensity variation with incident beam energy: on resonance (of both Fe and Ni), the order parameter follows the (001) peak intensity increase, with a concomitant decrease of the (002) peak. [24]

We begin our detailed discussion of the XRD results by considering scattering along the [001] direction. Misfit dislocations introduced into the layers as the films relax broadens the rocking curves with the Cu buffer layer showing a mosaic of about 2° in-plane. The subsequent $Cu_{100-x}Ni_x$ layers have lower mosaicity, which also decreases monotonically with increasing Ni content from 1.6° to 0.8° over the composition range $0 \leq x \leq 90$ at.%. The mosaicity

of the FeNi layer follows that of the CuNi layer on which it was deposited, although it is generally about 0.2° larger. Fig. 3 shows the diffracted intensity along the [001] direction with the sample aligned to the CuNi(002) peak for the 40 at.% Ni sample recorded using an energy of 7090 eV. The analysis is complicated by the presence of many overlapping reflections, so in order to extract meaningful data the experimental data were fitted to a series of Pearson7 functions [30], as shown by the lines in fig. 3 and fig. 4. An additional weak diffuse background peak was also observed around the 002 reflections which could only be resolved when the diffracted intensity was plotted on a logarithmic scale (fig. 3). Strong scattering is observed around the (002) position, Q_{002}, but we note the absence of the single (001) peak expected at $Q_{001} = Q_{002}/2$ for the $L1_0$ structure. Instead, two satellites, symmetrically placed on either side of the expected Q_{001}, are observed. These satellites arise from composition modulations along the [001] direction with a specific spatial periodicity Δd as described in detail previously [24]. Since these satellites are due to the symmetric chemical ordering along the growth direction they only appear at the 001 reflection and do not affect the intensity or shape of the 002 reflection. Tuning the incident radiation energy to the Fe K edge causes these satellite peaks to increase in intensity, as expected for the $L1_0$ structure. The inset in fig. 3 shows the satellites measured on resonance at 7120 eV on a linear scale. We note that most of our samples exhibit the two satellite reflections centered around the expected Q_{001} position. There were slight variations in the peak separation between samples ($2\Delta Q = 0.04 - 0.18(1)$ Å^{-1}), indicating small changes in the structural modulation wave-vector.This corresponds to a composition modulation period of $\Delta d = \frac{2\pi}{\Delta Q}$ of 69(1) Å for the least ordered sample grown on the 10 at.% Ni buffer layer. The most well ordered sample was grown on the 60 at.% Ni buffer layer and has a single non-split peak at the Q_{001} (see the inset in fig. 6). In this case the Q_{001} intensity was relatively strong compared to other samples, but a diffuse background was still observed, suggesting that, even for this sample, a small degree of chemical disorder remains probably arising from surface roughness or terrace steps on the surface of the buffer layer.

From the width of the diffraction peaks and using the Scherrer formula we can estimate the correlation length, ζ_z, of the crystalline regions. As we assume a pre-factor of 1 in the Scherrer equation, however, our values of ζ_z are likely to be underestimations. For the Cu buffer, ζ_z lies in the range 100 Å to 170 Å. These somewhat small correlation lengths, compared to the $\sim$ 1000 Å layer thickness, are probably due to the presence of strain fields in the sample. Similarly, for the CuNi layer ζ_z is in the range 165 Å to 205 Å and for FeNi it is slightly smaller; ζ_z =60–180 Å.

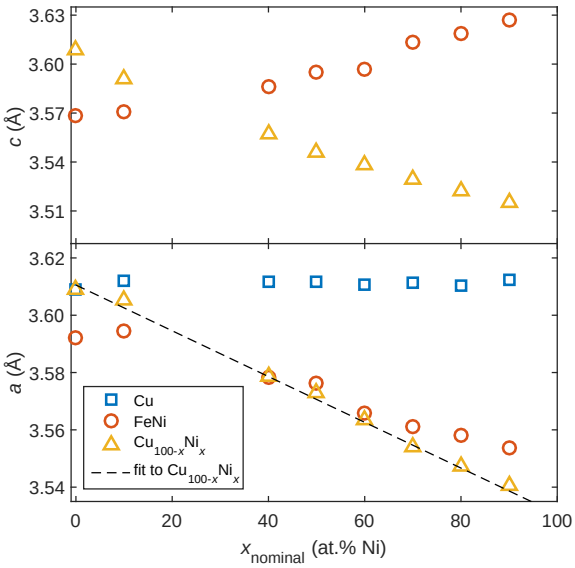

Figure 5. Lattice parameters out-of-plane (c, top) and in-plane (a, bottom) for each layer, vs the nominal Ni content of the CuNi buffer. The dashed line is a fit of a_{CuNi} vs x. Uncertainties are within the marker size.

Scans along different principal directions in reciprocal space were also performed to determine the tetragonality of the unit cells. Fig. 4 shows scans along the [001], [101] and [110] directions for the 40 at.% Ni sample recorded with an energy just below the Ni edge (8310 eV). Figs. 4 (a), (b) and (d) all contain three reflections which overlap; one from each layer which in order of increasing $|Q|$ arise from the Cu, $Cu_{100-x}Ni_x$ and FeNi. Energy dependent scans, whilst maintaining a fixed scattering vector, were used to confirm the origin of each peak whose position was determined by fitting Pearson7 functions. The fact that the (110) reflection shows no splitting confirms that the compositional modulation is along the [001] direction only and appears similar to data presented of Mizuguchi *et al.* [9] and Kojima *et al.* [10].

The a and c lattice parameters for the CuNi and FeNi layers were determined simultaneously from the fitted positions of *all* the available reflections from each layer using a χ^2 minimisation [31] and assuming a tetragonal unit cell. The in-plane lattice parameter a could be determined from the 202 and 220 scans which include in-plane directions. The Cu buffer was assumed to be cubic with the lattice parameter again determined from all the measured reflections. The lattice parameters for each layer as a function of nominal Ni content x of the $Cu_{100-x}Ni_x$ buffer are shown in fig. 5. The Cu lattice parameter a_{Cu} =3.611(1) Å is consistent with a relaxed bulk-like

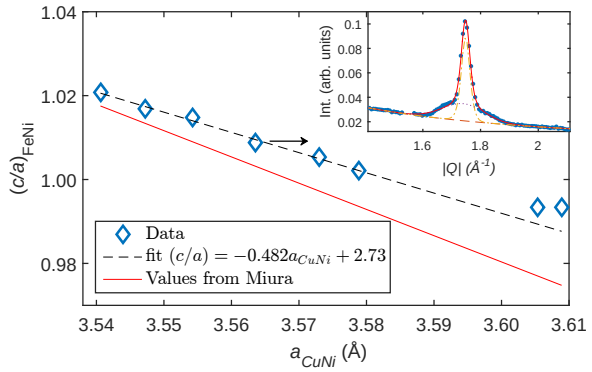

Figure 6. The c/a ratio for the FeNi layer, vs a_{CuNi}. The red line is the variation predicted by Miura [23]. The dashed line is a linear fit to the first 6 points. Inset is the scan over the 001 reflection for the most well-ordered sample. The lattice parameters and c/a of this sample are $a_{FeNi} = 3.566$ Å and $c/a = 1.009$, both are close to the ideal values. Uncertainties are within the marker size.

layer and was the same in all samples. The CuNi buffers show a slight tetragonality with $c_{\mathrm{CuNi}} \leq a_{\mathrm{CuNi}}$, and both a_{CuNi} as well as c_{CuNi} vary linearly with nominal x as expected from Vegard's law. The in-plane parameter of the FeNi layers, a_{FeNi}, also varies linearly with the buffer's nominal Ni concentration x. However, as the slopes of a_{FeNi} and a_{CuNi} versus nominal x are different, there is some additional in-plane relaxation within the FeNi layers. For a CuNi buffer of 40 at.% Ni $a_{\mathrm{FeNi}} = a_{\mathrm{CuNi}}$ and the L1$_0$ NiFe adopts its fully relaxed value. Buffers layers with other compositions cause some strain to be imparted into the FeNi layer, but with some relaxation towards its bulk value. The relaxation mechanism remains unclear, but for CuNi buffer layers with $x \leq 40$ at.% Ni the FeNi layer is tensile strained in the plane whilst for $x = 50$ at.% Ni and higher it is compressively strained in the plane. The out-of-plane FeNi parameter c_{FeNi} increases with the decreasing a_{FeNi} over the entire Ni concentration range, with the unit cell volume being approximately constant at $a^2_{\mathrm{FeNi}} c_{\mathrm{FeNi}} \approx 45.86(3)$ Å^3 which compares favourably with the theoretical volume for L1$_0$, $V_{\mathrm{FeNi}} = 45.37$ Å^3 [5]

To highlight the strain introduced into the FeNi film by the CuNi buffer layer composition, we plot the c/a ratio of the FeNi layers as a function of a_{CuNi} in fig. 6. A linear decrease with a_{CuNi} is observed as would be expected from volume conservation of the FeNi unit cell. The two samples with FeNi with $c/a < 1$ (with a low Ni content in the buffer fig. 5) clearly deviate from this linear behaviour and so the two points with $a_{\mathrm{CuNi}} > 3.6$ Å have not been included in the dashed fitted line shown in fig. 6. The calculation by Miura *et al.* [23], which assumes $a_{\mathrm{FeNi}} = a_{\mathrm{CuNi}}$, is also shown by the solid line in fig. 6. Compared to these theoretical values, the tetragonality in our samples are somewhat larger which is probably due to the slight relaxation of the FeNi film causing dislocations at the FeNi and CuNi interface and only a partial coupling of the in-plane parameters (i.e. $a_{\mathrm{FeNi}} \neq a_{\mathrm{CuNi}}$ - fig. 5). Our most well ordered sample, without any splitting of the (001) reflection (as shown in the inset of fig. 6), has $a_{\mathrm{FeNi}} = 3.566(3)$Å and $(c/a)_{\mathrm{FeNi}} = 1.009(2)$. These values are within uncertainty of the theoretical values for L1$_0$ FeNi ($a = 3.56$ Å and $c/a = 1.006$) [5] and similar to those reported by Miura [23] - $a_{\mathrm{FeNi}} = 3.556$ Å and $(c/a)_{\mathrm{FeNi}} = 1.008$.

3.2. Magnetic properties

The magnetic properties of the films were determined from in- and out-of-plane hysteresis loops measured by SQUID at 300 K. To enable comparison with our previous results [24], the saturation magnetization was also measured at 35 K for the $x = 60$ at.% sample, and was found to be about 6 % larger than at 300 K. The same enhancement at low temperature is expected for all other samples, but has not been compensated for in the results presented herein. Since the critical temperature of $Cu_{100-x}Ni_x$ is above room temperature for compositions above $x = 60$ at.%, there is a weak contribution from this layer in the total magnetic signal measured in the SQUID. To isolate the FeNi signal, the magnetic moment from the buffer layer was compensated for by using measurements from Si/Cu/CuNi reference samples with identical buffer layer thickness and with the CuNi buffer layers having a Ni content, x, of 40, 60, 70 and 80 at.%. Any effects of different strain states in the CuNi layers induced by the FeNi overlayers was assumed to have a negligible impact on the measured magnetization of the reference samples. A linear extrapolation was used to estimate the signal from a 90 at.% CuNi buffer layer. For the x =40 at.% sample, only the diamagnetic background remained. Thus, for trilayers with CuNi buffer layers with $x \leq 50$ at.% Ni, a standard linear background subtraction was sufficient to isolate the the FeNi signal.

After compensating for the background signals from the buffer layers, the effective anisotropy K_{eff} was calculated by integrating the area between the M-axis and the out-of-plane loop, since the in-plane $M(H)$ loop was square for all samples. The uniaxial anisotropy energy contribution K_{U} was obtained via the relationship $K_{\mathrm{U}} = K_{\mathrm{eff}} - K_{\mathrm{shape}}$ and assuming the shape anisotropy was dominated by the finite extent of the film, $K_{\mathrm{shape}} = -\mu_0 M_S^2/2$ with M_S being the saturation magnetization [32]. Under these assumption, $K_{\mathrm{eff}} < 0$ favours in-plane macroscopic magnetization and $K_{\mathrm{U}} > 0$ implies out-of-plane

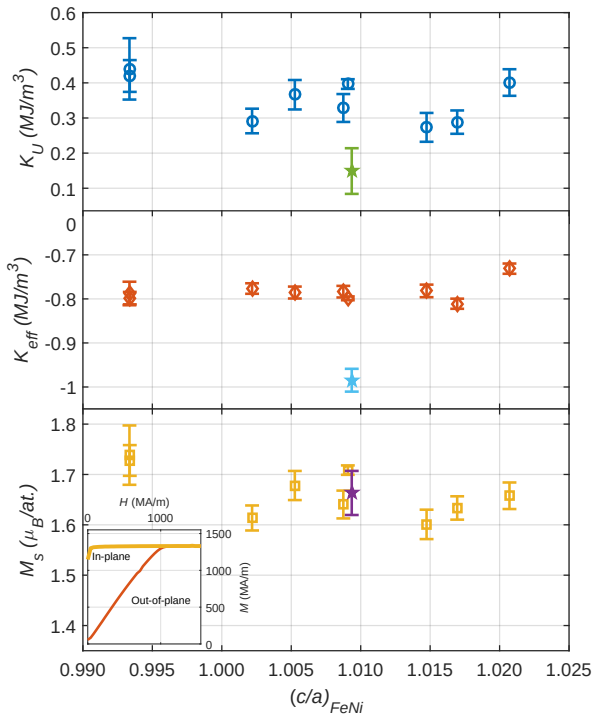

Figure 7. Dependence on $(c/a)_{\mathrm{FeNi}}$ of the saturation magnetization M_{S} (bottom), effective anisotropy energy K_{eff} (centre) and uniaxial anisotropy energy K_{U} (top), as extracted from SQUID measurements at 300 K. For comparison with the L1$_0$ data the stared symbol in each panel is the data recorded from the disordered A1 sample. Inset in the bottom panel: Half magnetisation loops recorded along in- and out-of-plane directions for the 60 at.% Ni buffered sample.

uniaxial anisotropy. We plot the experimentally determined saturation magnetisation, M_{S}, and the anisotropy energies, K_{U} and K_{eff}, as a function of $(c/a)_{\mathrm{FeNi}}$ in fig. 7. K_{eff} shows an almost constant effective in-plane anisotropy at about -0.8 MA/m for all samples, but nevertheless a positive uniaxial anisotropy contribution. As K_{eff} is invariant with $(c/a)_{\mathrm{FeNi}}$, the variation in K_{U} mimics the observed changes in M_{S}. The exception is the A1 reference sample (indicated by a star in the plot) which has a smaller K_{U} than the L1$_0$ samples. The reported value for the A1 phase is likely to be overestimated, since the saturation field for this particular sample was so high that it was difficult to reach in the SQUID.

Neither K_{U} nor M_{S} show any strong dependence on $(c/a)_{\mathrm{FeNi}}$ although any variation within this strain range is theoretically predicted to be small and well within our experimental uncertainties. Our values of $K_{\mathrm{U}} \sim 0.35\,\mathrm{MJ\,m^{-3}}$ are smaller than that predicted for the L1$_0$ phase of FeNi ($\sim 0.56\,\mathrm{MJ\,m^{-3}}$) [23] but larger than FeNi films grown on only a Cu buffer layer ($K_{\mathrm{U}}^{\mathrm{Cu}}$ <0.2 MJ/m^3) [24]. Our values are not, however, as large as reported by others [8, 10]: $K_{\mathrm{U}} = 0.8 - 0.9\,\mathrm{MJ/m^3}$, but are similar to films deposited on CuNi ($0.5\,\mathrm{MJ\,m^{-3}}$) [9]. The effect of the observed chemical disorder in the form of composition modulations is not clear. Creating composition modulations with well defined out-of-plane wave-vectors could be a way to relieve strain along the out-of-plane [001] direction, but this adds a small degree of disorder, and further theoretical models are needed to understand how this may effect the anisotropy.

We can estimate the chemical composition of the FeNi layer by comparing the saturation magnetisation with the Slater-Pauling curve at 0 K [33]. The saturation magnetisation is expected to be 1.7 μ_{B}/at. for a $Fe_{50}Ni_{50}$ alloy. As the magnetisation data were recorded at 300 K we need to compensate for the 6 % reduction in the moment to compare with the Slater-Pauling curve. The corrected moments are slightly larger than the ideal 1.7 μ_{B}/at. showing that the FeNi layers are slightly Fe rich in our samples covering the range 50(1)–57(1) at.% Fe. This composition range is, however, well within the composition range (51–71 at.% Fe) where the FeNi L1$_0$ phase formation is possible [34]. Small drifts in the deposition rates in our chamber could account for the composition being slightly away from the ideal Fe_{50}:Ni_{50}. The variation in M_{S} is correlated directly with the variation in ΔQ showing that the splitting of the (001) diffraction peak is related directly to the composition, as suggested previously [24].

4. Conclusions

We have successfully fabricated FeNi in the L1$_0$ phase by magnetron sputtering on HF-etched Si substrates using $Cu/Cu_{100-x}Ni_x$ buffers. The strain within the L1$_0$ FeNi layer, $(c/a)_{\mathrm{FeNi}}$, was varied from compressive to tensile in a continuous and controlled manner through the composition of the $Cu_{100-x}Ni_x$ buffer layer over the range $0 < x < 90$. A simple linear dependence between a_{FeNi} and a_{CuNi} was observed which allows the strain in the FeNi over layer to be engineered easily. For a L1$_0$ FeNi film deposited on a $x = 60$ at.% CuNi buffer layer a single (001) diffraction peak was observed with lattice parameters and tetragonality within error of the ideal values for L1$_0$ FeNi. A splitting of the (001) peak, which displayed the expected resonant behaviour, was observed in all other samples which we attribute to compositional modulations along the [001] direction only. The uniaxial anisotropy energy K_{U} is positive and larger than observed in our previous study on FeNi films grown on pure Cu buffers [24] and comparable with other literature examples. The independence of K_{U} with $(c/a)_{\mathrm{FeNi}}$ shows that L1$_0$ FeNi films can be readily incorporated into epitaxial heterostructures without deleterious impact on its

magnetic properties. It may be possible to engineer still larger strains into a $L1_0$ FeNi film through choice of different virtual substrate but care will be needed to avoid interface roughness if the epitaxial mismatch is too high.

The authors acknowledge the financial support of the UK-EPSRC and the Swedish Research Council (VR) as well as ABB AB. We acknowledge the European Synchrotron Radiation Facility for provision of synchrotron radiation facilities and we would like to thank Simon Brown for his assistance and insight. XMaS is a mid-range facility supported by EPSRC and we are indebted to the whole XMaS team for invaluable support during beamtime.

References

[1] Coey J 2009 *Magnetism and Magnetic Materials* (Cambridge University Press)
[2] Kramer M J, McCallum R W, Anderson I A and Constantinides S 2012 *JOM* **64** 752–763
[3] Coey J 2012 *Scripta Materialia* **67** 524–529
[4] Ronning F and Bader S 2014 *Journal of Physics: Condensed Matter* **26**
[5] Edström A, Chico J, Jakobsson A, Bergman A and Rusz J 2014 *Physical Review B* **90** 014402 (*Preprint* `arXiv:1404.7097v1`)
[6] Lewis L H, Mubarok A, Poirier E, Bordeaux N, Manchanda P, Kashyap A, Skomski R, Goldstein J, Pinkerton F E, Mishra R K, Kubic Jr R C and Barmak K 2014 *Journal of Physics: Condensed Matter* **26** 064213
[7] Lewis L H, Pinkerton F E, Bordeaux N, Mubarok A, Poirier E, Goldstein J I, Skomski R and Barmak K 2014 *IEEE Magnetics Letters* **5** 5500104
[8] Poirier E, Pinkerton F E, Kubic R, Mishra R K, Bordeaux N, Mubarok A, Lewis L H, Goldstein J I, Skomski R and Barmak K 2015 *Journal of Applied Physics* **117** 17E318
[9] Mizuguchi M, Kojima T, Kotsugi M, Koganezawa T, Osaka K and Takanashi K 2011 *Journal of the Magnetics Society of Japan* **35** 370–373
[10] Kojima T, Ogiwara M, Mizuguchi M, Kotsugi M, Koganezawa T, Ohtsuki T, Tashiro T Y and Takanashi K 2014 *Journal of Physics: Condensed Matter* **26** 064207
[11] Kotsugi M, Maruyama H, Ishimatsu N, Kawamura N, Suzuki M, Mizumaki M, Osaka K, Matsumoto T, Ohkochi T, Ohtsuki T, Kojima T, Mizuguchi M, Takanashi K and Watanabe Y 2014 *Journal of Physics: Condensed Matter* **26** 064206
[12] Bordeaux N, Montes-Arango A M, Liu J, Barmak K and Lewis L H 2016 *Acta Materialia* **103** 608–615
[13] Néel L, Pauleve J, Pauthenet R, Laugier J and Dautreppe D 1964 *Journal of Applied Physics* **35** 873
[14] Paulevé J, Chamberod A, Krebs K and Bourret A 1968 *Journal of Applied Physics* **39** 989
[15] Reuter K, Williams D and Goldstein J 1988 *Geochimica et Cosmochimica Acta* **52** 617–626
[16] Lee S, Edalati K, Iwaoka H, Horita Z, Ohtsuki T, Ohkochi T, Kotsugi M, Kojima T, Mizuguchi M and Takanashi K 2014 *Philosophical Magazine Letters* **94** 639–646
[17] Makino A, Sharma P, Sato K, Takeuchi A, Zhang Y and Takenaka K 2015 *Scientific Reports* **5** 16627
[18] Shima T, Okamura M, Mitani S and Takanashi K 2007 *Journal of Magnetism and Magnetic Materials* **310** 2213–2214
[19] Sakamaki M and Amemiya K 2014 *Journal of Physics: Condensed Matter* **26**
[20] Futamoto M, Nakamura M, Ohtake M, Inaba N and Shimotsu T 2016 *AIP Advances* **6** 085302
[21] Ohtake M, Itabashi A, Kirino F and Futamoto M 2013 *IEEE Transactions on Magnetics* **49** 3295–3298
[22] Andreazza P, Pierron-Bohnes V, Tournus F, Andreazza-Vignolle C and Dupuis V 2015 *Surface Science Reports* **70** 188–258
[23] Miura Y, Ozaki S, Kuwahara Y, Tsujikawa M, Abe K and Shirai M 2013 *Journal of Physics: Condensed Matter* **25** 106005
[24] Frisk A, Lindgren B, Pappas S D, Johansson E and Andersson G 2016 *Journal of Physics: Condensed Matter* **28** 406002
[25] Pappas S D, Kapaklis V, Delimitis A, Jönsson P E, Papaioannou E T, Poulopoulos P, Fumagalli P, Trachylis D, Velgakis M J and Politis C 2012 *Journal of Applied Physics* **112** 053918
[26] Brown S, Bouchenoire L, Bowyer D, Kervin J, Laundy D, Longfield M, Mannix D, Paul D, Stunault A, Thompson P, Cooper M, Lucas C and Stirling W 2001 *J. Sync. Rad.* **8** 1172–1181
[27] Busing W R and Levy H A 1967 *Acta Crystallographica* **22** 457–464
[28] Vaz C, Steinmuller S, Moutafis C, Bland J and Babkevich A 2007 *Surface Science* **601** 1377–1383
[29] Cullity B D 1978 *Elements of X-ray Diffraction* 2nd ed Addison-Wesley series in metallurgy and materials (Reading: Addison-Wesley Publishing Company)
[30] Birkholz M 2006 *Thin Film Analysis by X-ray Scattering* (Weinheim: Wiley-VCH)
[31] Hughes I G and Hase T P 2010 *Measurements and their Uncertainties* (New York: Oxford University Press)
[32] Johnson M T, Bloemen P J H, Broeder F J a D and Vries J J D 1996 *Reports on Progress in Physics* **59** 1409–1458
[33] Crangle J and Hallam G 1963 *Proceedings of the Royal Society of London A* **272** 119–132
[34] Reuter K, Williams D and Goldstein J 1989 *Metallurgical Transactions A* **20** 711–718